CLM-P626

CLM-P626

UKAEA

Preprint

SPECTROSCOPY OF LASER FUSION PLASMAS

N. J. PEACOCK

CULHAM LABORATORY
Abingdon Oxfordshire

1980

CLM-P 626

SPECTROSCOPY OF LASER FUSION PLASMAS

N J Peacock
Culham Laboratory, Abingdon, Oxon, OX14 3DB, UK
(Euratom/UKAEA Fusion Association)

ABSTRACT

This paper surveys the parameters, such as density temperature, charge state and the appropriate scale lengths which characterise the extreme pressure conditions created by laser-irradiation of solid surfaces. Some differentiation is made between single beam irradiation of plane targets and multi-beam compression experiments.

Diagnostic techniques based on spectroscopic analyses of the X-ray and XUV emission is described in some detail. In this context are measurements of the electron temperature and electron energy transport, the ion mass motion and the particle densities from line intensities and from line shapes. Radiation transport, which is important in both emission and absorption studies is discussed in the derivation of $\langle \rho r \rangle$, the product of the plasma scale length and ion density. Novel measurement techniques yielding adequate space ($\gtrsim$ 1μm) and time ($\ll$ 1nsec) resolution of the spectrum are described.

Of more basic interest is the use of laser-produced plasmas for atomic structure studies of highly-ionised atomic species, line broadening and collective processes associated with extreme plasma conditions. "State of the Art" research programmes on these topics are discussed.

(Paper presented at the Physics of Ionised Gases 10th Summer School and Symposium, Dubrovnik, 25-29 August 1980)

November 1980
cms

Contribution for SPIG '80 Meeting at Dubrovnik, Yugoslavia, August 1980

SPECTROSCOPY OF LASER FUSION PLASMAS

N J Peacock
Culham Laboratory, Abingdon, Oxon, OX14 3DB, UK
(Euratom/UKAEA Fusion Association)

1. INTRODUCTION

Interest in the irradiation of solid targets by intense laser light stems from a number of topical research programmes which include (a) the absorption of laser light and the physical processes which lead to plasma heating: (b) the extension of laboratory plasma parameters to extremes of density $n_e \gtrsim 10^{24}\,cm^{-3}$, and of kinetic pressure, $n_e\,kT_e \sim 10^8 \rightarrow 10^9$ atmospheres: (c) the collective (non-linear) behaviour of plasmas in intense EM fields: (d) the generation of highly stripped ions and of multi-megagauss fields: (e) controlled fusion research. Spectroscopic measurements and analyses play an important part in all of these fields of study.

This paper sets out first of all to survey the parameters of density, n_e, temperature T_e, charge state Z_{eff}, and scale length $\left(n_e^{-1}\frac{\partial n_e}{\partial r}\right)^{-1}$ which characterise the extreme pressure conditions created in laser irradiation experiments. Differentiation is necessarily made between single beam irradiation of plane targets and plasma convergence (compression) experiments using multi-beam radially-symmetrical irradiation since only in the latter case can the very highest densities, $n_e \gtrsim 10^{24}\,cm^{-3}$, be reached.

Diagnostic techniques based on spectroscopic analyses of the X-ray and XUV emission is described in some detail. In this context are measurements of the electron temperature, the ion mass motion and the particle densities from emission line shapes and from line intensities. Radiation transport which is important in both emission and absorption studies is discussed, in Sections 3 and 4, in the derivation of $\langle \rho r \rangle$ the product of plasma scale length x density. Measurement techniques yielding adequate space resolution ($\gtrsim 1\mu m$) and time resolution ($\ll$ 1nsec) of the spectrum are treated in Section 5.

Of more basic interest, Section 6 is the use of laser-produced plasmas for atomic structure studies of highly-ionised atomic species and of appropriate rate coefficients and collective processes associated with extreme plasma conditions. "State of the art" research programmes on these topics are discussed.

2 PLASMA PARAMETERS PRODUCED IN LASER-FUSION EXPERIMENTS

In solid target irradiation experiments we expect the plasma generated at the surface of the target material to have profiles $n_e(r)$, $T_e(r)$ which are determined mainly by the laser wavelength λ_o, the intensity Φ_o and the duration τ_L of the irradiation pulse. Other factors such as laser bandwidth, angle of incidence and polarisation state are pertinent to the problem but for the sake of brevity these secondary factors are ignored in this discussion.

Penetration of the light beam and its interaction with the plasma is confined to a density region at or below the critical density for reflection, given by

$$n_{ec}\,\lambda_o^{\,2} = 1.12 \times 10^{13}\,\mathrm{cm}^{-1} \qquad (1)$$

For a 1μm output (neodymium) laser this region is $n_{ec} \lesssim 10^{21}\,\mathrm{cm}^{-3}$ while for a 10μm wavelength (CO_2) laser $n_{ec} \lesssim 10^{19}\,\mathrm{cm}^{-3}$.

In the simplest case of classical resistive absorption, Dawson and Oberman (1962), Dawson (1964), $T_e(r)$ and $n_e(r)$ are approximately as predicted in Fig.1 by the 1D Medusa numerical code, Christiansen et al (1974).

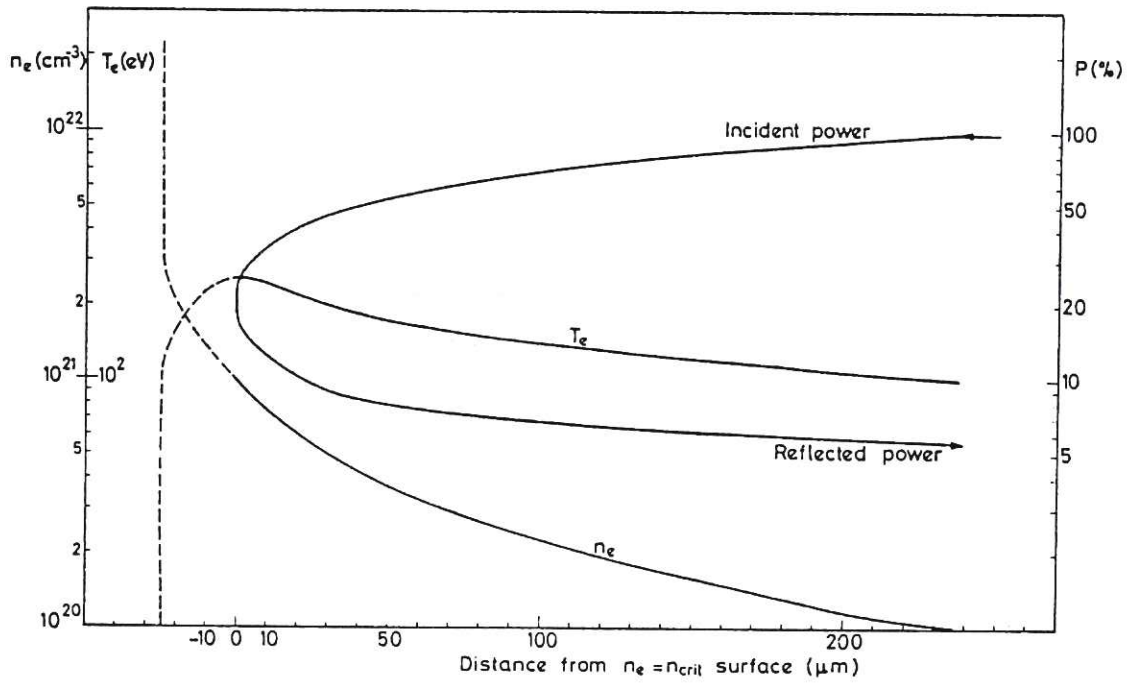

FIG.1 Time-averaged, density and temperature profiles along the normal to a polyethylene surface irradiated by a 4.5ns long pulse of 1μm light with a peak intensity of $10^{12}\mathrm{Wcm}^{-2}$. Predictions were made using the 1-D MEDUSA code assuming classical resistive absorption of the incident intensity. GALANTI et al (1974).

This example refers to 1μm irradiation of a $(CH_2)_n$ target with a flux intensity $\Phi_o = 10^{12}$ W cm^{-2}. Resistive absorption is a common enough situation with higher Z targets over a wider range of light flux intensity. A consideration of the energy balance, Galanti et al (1974), shows that most of the input energy is accounted for by free expansion of the plasma from the target and, in the case of non-hydrogen targets, radiation loss. Only a relatively small fraction, typically a few per cent of the incident energy appears as thermal, $n_e kT_e$, energy in the plasma. Galanti and Peacock (1975) find the relationship,

$$kT_e(\text{eV}) = 6 \times 10^{-6} \phi_A^{2/3} \qquad (2)$$

with ϕ_A the intensity in W cm^{-2} absorbed in the plasma.

At a much higher flux intensity than applies to Fig.1, the 'quiver' velocity of the electrons in the laser field,

$$\tilde{v}(\text{cm s}^{-1}) = \frac{eE_o}{m\omega_o}$$

$$= 25\, \lambda(\mu\text{m})\, \Phi_o^{1/2}(\text{W cm}^{-2}) \qquad (3)$$

is sufficiently high to modify the electron thermal velocity. As a consequence, non-linear coupling processes such as stimulated Brillouin backscatter, profile steepening due to light pressure and acceleration of particles can occur and impair the energy coupling to the thermal component of the plasma. The theoretical treatment and experimental evidence for these phenomena are surveyed by Hughes (1979), Kruer (1979) and Key (1979). The velocity distribution departs from Maxwellian and develops typically a high energy component with a 'temperature' given by

$$T_{eh}(\text{eV}) \propto (\Phi\lambda_o^2)^{\delta} \qquad (4)$$

where $\Phi_o\lambda_o^2$ has units of W μm²/cm² and $\delta \simeq 0.7$ for $\Phi_o\lambda_o^2 < 10^{15}$ while for $\Phi_o\lambda_o^2 > 10^{15}$, $\delta \simeq 0.25$. It is to be noted, eqs(3) and (4), that T_{eh} is proportional to the 'quiver' electron energy in the laser field. Resonance absorption, although not a non-linear process, appears to be an effective mechanism for light absorption even with near-normal incidence irradiation and almost irrespective of its polarisation. When coupled with the pondermotive force due to the light pressure, which can reach Mbars in high intensity irradiation experiments, $P_{h\nu}$ (Mbar) $= \Phi_o/c = 3 \times 10^{-16}\Phi$(W cm^{-2}),

resonance absorption allows the light energy to be dumped at the critical density and, unfortunately, transferred not to the thermal component of the plasma but to acceleration of electrons. An example of density profile steepening, due to the light pressure carving out a hollow in the density gradient, is shown in Fig.2 for a Nd-laser irradiated microballoon.

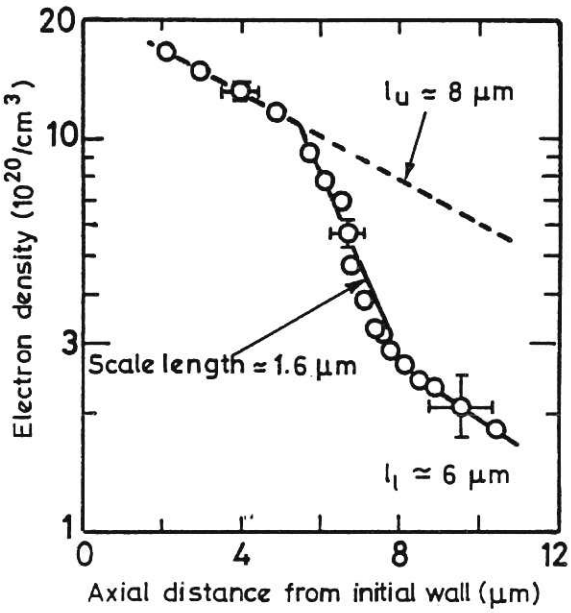

FIG.2 Electron density profile of the surface plasma from a 41μm glass shell irradiated by a 30ps pulse of 1μm laser light with an intensity of 300TW/cm^2 ℓ_u and ℓ_ℓ are the super- and sub-critical density scale lengths. The self-steepened density gradient illustrates the effects of the radiation pressure of the incident laser beam. ATTWOOD (1978).

Transport of energy into the target material from the critical surface is a complex problem and depends largely on the 'collisionality' of the plasma at and above the critical density. Stated another way, the manner of energy transport depends on the mean free path of the particles relative to the density and temperature scale lengths. Energy can be conveyed by several physical mechanisms e.g. by heat conduction, which may be limited by the number of available electrons, by ion acoustic turbulence or by electric fields or even by self-generated (i.e. thermo-electric) magnetic fields. The scale length for heat propagation is

$$\ell_H^2 = \frac{10^{20}\, T_e^{5/2}\, \tau}{Z(1 + 1/Z)\, n_e} \qquad (5)$$

Alternative and competing energy transport is by shock waves, with a velocity $V_s = [(ZkT_e + kT_i)/M]^{1/2}$, by fast electron 'preheat' and by X-ray radiation transport. In high intensity irradiation experiments shock propagation into the near solid material overtakes the thermal conduction front after about 0.1nsec, so that for laser pulse durations $\tau \gtrsim$ 1ns a hydrodynamic model of the energy balance is appropriate, Key (1979).

A schematic diagram of the absorption of light energy, its redistribution and its effect on the density and temperature profiles is illustrated in Fig.3. This diagram is appropriate to 1μm wavelength irradiation of a 100μm diameter spherical shell with $\Phi_o \sim 10^{15}$ W cm^{-2}. A suprathermal

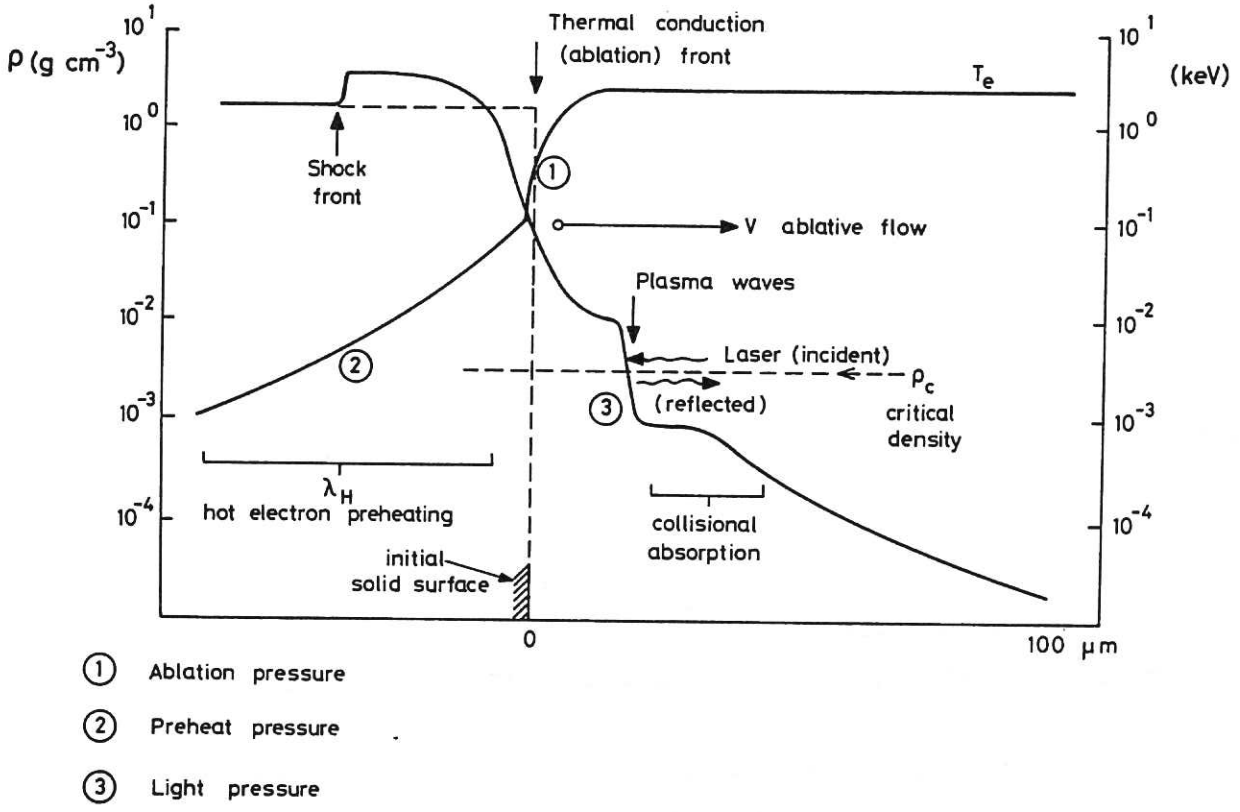

FIG. 3 Schematic of the spatial variation of the density ρ and electron temperature T_e during steady state irradiation of a 100μm diameter solid target with a 1μm laser, intensity 10^{15}W cm^{-2}. λ_H is the scale length for hot electron preheating within the shell. After KEY (1979).

electron energy component, $T_{eh} \sim 10$ keV, eq(4) is typical in such experiments and has a deposition length of the order of 10's of microns in the solid. This deposition can itself generate plasma pressures above a Mbar, the plasma having relatively low temperature but with a density close to that of a solid, Fig.3. Long wavelength, infra red lasers, such as the CO_2 laser, are so efficient at generating suprathermal electrons that the hot electron transport can be considered as a surrogate 'driver' in these material compression experiments.

A discussion on plasma profiles is not out of context in a spectroscopic paper since these have important consequences in the calculation of emission and absorption line shapes, in the prediction of the degree of ionisation and in the thermodynamic (non-equilibrium) state of the plasma.

Assuming the relation given in eq(2) to hold and that the ionisation potential is given by a functional relation viz.

$$\psi_z \propto RyZ^{\alpha} \propto AT_e$$

with $\alpha \sim 2$ and A typically between 3 and 10, then it would appear that with a fixed laser frequency an increase in the flux intensity Φ_o might be effective in raising the charge state Z.

Ionisation is most efficiently carried out by thermal electron collisions in plasma regions where the temperature and density are high and where the ions have a relatively long ionisation time (the last being equated with a relatively large plasma dimension). In practice, as we have seen, both the fractional thermal energy component and the scale lengths in the laser plasma interaction decrease as the irradiation becomes more intense. The coupling processes become increasingly more profligate in sustaining energy loss processes by reflections and by acceleration of particles. As a result the charge state only weakly increases with light intensity on the target surface. Because of the steepened gradients, non-stationary ionisation balance conditions are more likely.

The use of higher frequency lasers operating in the visible or UV might prove a more effective route to the production of stationary ionisation and highly charged ion states since the primary light energy is deposited at a higher critical density.

In general terms, a stationary state will be reached within a scale length ℓ_s determined by the slowest rate process, usually recombination i.e.

$$\ell_s = \frac{V_{iz}}{n_e \alpha (n_e, T_e, \psi_z)} \qquad (6)$$

where V_{iz} is the escape velocity of the ions which will be approximately equal to their thermal speed. Appropriate recombination rates $\alpha(n_e, T_e, \psi_z)$ have been calculated by Donaldson (1976), see e.g. Fig.4. For a highly charged Ti ion plasma at $n_e = 10^{21} cm^{-3}$ the dielectronic rate is negligible compared to collisional radiative recombination α_{CR}, while even for low charge states as in carbon plasmas the dielectronic contribution is only important for $n_e \gtrsim 10^{19} cm^{-3}$. Inserting into eq(6) values of $\alpha_{CR} \sim 10^{-11} \rightarrow 10^{12} cm^{+3} s^{-1}$, typical values for $V_{iz} \simeq 2 \times 10^{7} cm\ s^{-1}$ and $n_e \sim 10^{21} cm^{-3}$,

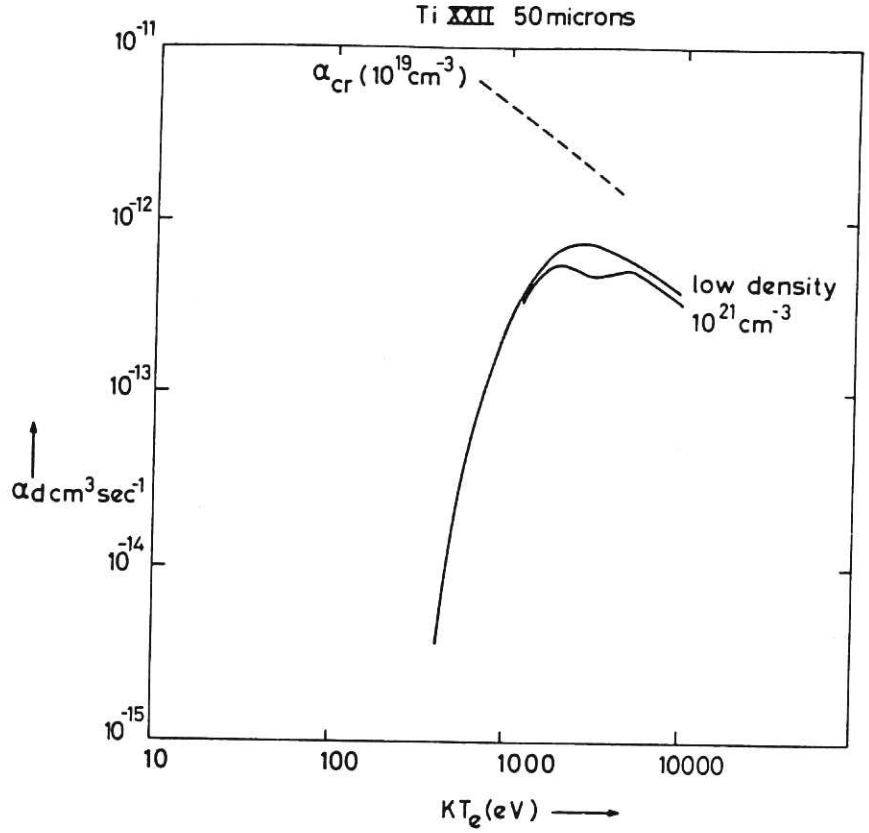

FIG.4 Dielectronic recombination coefficient, α_d (full line), and collisional radiative recombination coefficient, α_{CR} (dashed line), as a function of temperature and density. Equilibrium conditions of the ion species assumed in a Ti plasma with a scale length of 50μm. Line opacity and collisional de-excitation are included in the calculations, DONALDSON (1976).

we see that steady state conditions are reached for $\ell_s \gtrsim 20 \rightarrow 200\mu m$. On the simple theoretical model that only the heat conduction scale length eq(5), determines the value of ℓ_s, Colombant and Tonon (1973), then one could expect stationary ionisation conditions given by $n_e \tau_{ion} = \frac{1}{\alpha(Z+1) + S(Z)}$, where α and S are the recombination and ionisation coefficients. In experiments to investigate the question of ionisation-recombination balance Galanti and Peacock (1975), Zigler et al (1979) and Boiko, Chugunov et al (1979) typically find non-stationary ionising conditions near the critical density surface. The first of these authors evaluate $n_e \tau_{ion} = n_e \ell_s / V_{iz} \sim 10^{10} cm^{-3} s$.

In the freely expanding plasma ablated from the critical density surface the ionic populations are very far from ionisation-recombination equilibrium. This results from the rapid decrease in density due to free expansion rather than due to the relatively slow recombination at distances 10's or 100's of microns from the critical surface. An illustration of the effect of non stationary ion populations is seen in Fig.5 where the

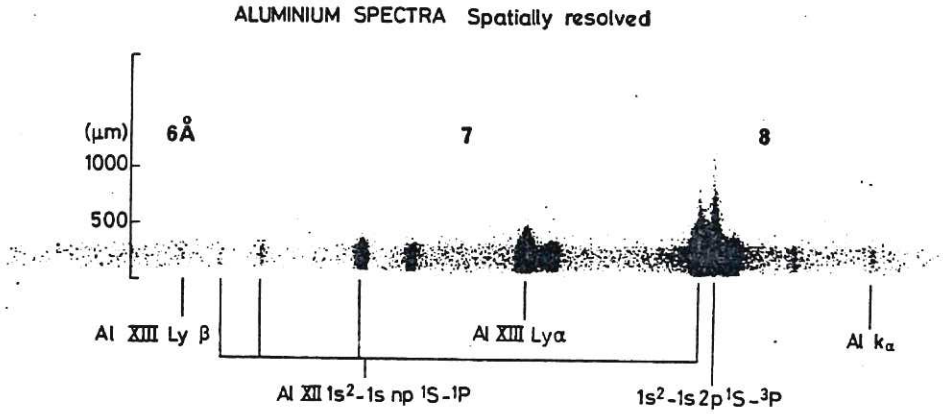

FIG.5 Space-resolved spectrum from a laser-irradiated plane aluminium target. Distances (μm) are measured from the target surface.

intercombination line intensity of AlXII exceeds its neighbouring allowed line intensity at 500μm or more from the target surface. This reversal of the stationary state intensity ratio results from the preferential population of the n=2 triplet levels relative to the singlet levels in the conditions of a rapidly recombining Al^{+12} plasma. Optical opacity of the allowed line could in principle cause the intercombination line to assume an apparently higher intensity but such an explanation can be discounted in the case of the expanding plasma since line opacity decreases with distance from the target surfaces.

3 ANALYSIS OF THE EMISSION SPECTRA FROM LASER-IRRADIATED SOLID TARGETS

The EM emission from plasmas produced by high intensity laser irradiation of solids typically accounts for several % or more of the input energy and lies predominantly in the X-ray and XUV spectral regions. A spectrum of the emission from an irradiated glass microballoon is shown schematically in Fig.6. Superimposed on the continuum are the resonance lines from highly-ionised atoms of the irradiated shell. These line features are mainly due to K and M shell excitation of ions isoelectronic with elements of the first two periods and are often used as diagnostic indicators of such parameters as the ablation pressure, the expansion and compression velocity, the density and $\int \rho . dr$.

Analyses of the line intensities specifically for density derivation has been surveyed by Boiko, Pikuz and Faenov (1979) and Peacock (1980). Articles by Vinogradov, Sobelman and Yukov (1974), Doschek et al (1975), Peregudov et al (1978) and by Galanti and Peacock (1975) all refer to diagnostic measurements in laser-produced plasmas using line intensity ratios.

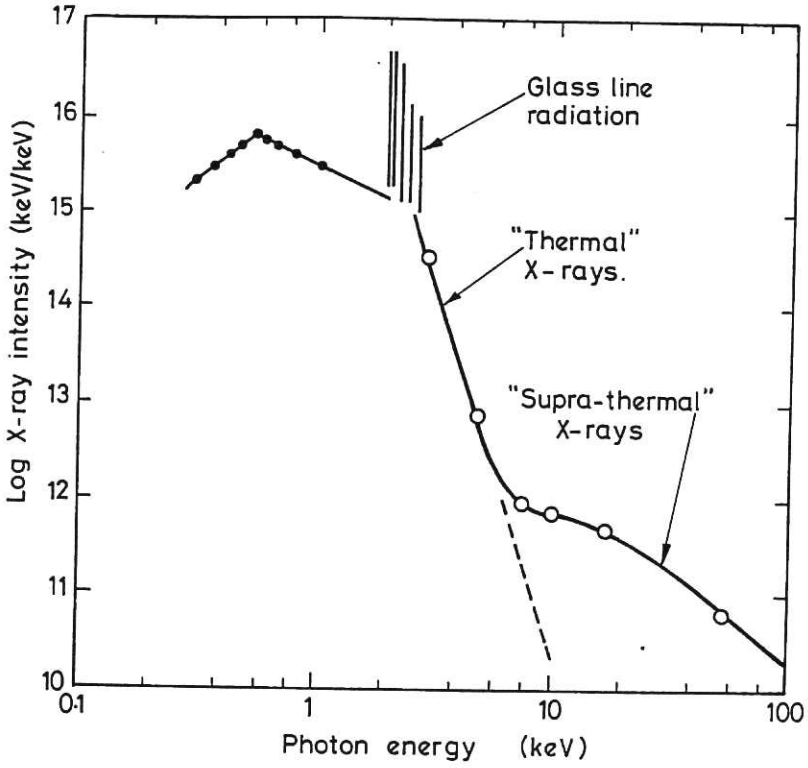

FIG.6 Time- and space-integrated X-ray emission spectrum from a laser-irradiated microballoon target. ATTWOOD (1978).

However, the usefulness of these measurements based on line intensity ratios is somewhat limited due to the dynamic motion of the laser-produced plasma, the complexity of its density and temperature profiles, the probability of non-stationary ionisation balance and finally, optical opacity. As pointed out by Peacock (1979) most of the simplified models of the line ratios fail to match the experimental conditions, the assumption of optical thinness often limiting their application to $n_e \lesssim n_{ec}$. Visible light interferometry, however, Section 4, is a more appropriate technique for evaluating density in this density range.

In contrast, line profile analysis offers quite unique information and has been used with some success, provided that radiation transport is properly taken into account, in the determination of the values of density ($n_e \lesssim 10^{24} m^{-3}$) and of $\int \rho . dr$ which obtain in the plasma core of laser driven experiments. In this respect it is pertinent, before discussing experimental line shapes, to discuss the problem of opacity in bound-bound transitions.

3.1 Optically Thick Line Emission

For the sake of simplicity we deal in the first instance with the intensity emerging from a homogeneous plasma of depth x = D,

$$\frac{dI(\nu,x)}{d\tau(\nu)} = I(\nu,x) - S(\nu,x) \qquad (7)$$

where $S(\nu)$, the source function, is the ratio of the emissivity $\varepsilon(\nu)$, to the absorption coefficient $a(\nu)$, and $a(\nu)dx = d\tau(\nu)$ is the incremental optical depth.

The solution of equation (7) is of the form,

$$I(\nu) = \frac{\varepsilon(\nu)}{a(\nu)} \left[1 - e^{-\tau(\nu)}\right] \qquad (8)$$

and

$$\tau(\nu) = \int_{o}^{D} N_z(x) L(\nu) \frac{h\nu_o}{4} B_{\ell,u} . dx \qquad (9)$$

where $B_{\ell,u}$ is the Einstein absorption coefficient and $L(\nu)$ is the absorption line shape factor which when integrated over the profile gives unit probability of absorption. $L(\nu)$ is a function of the intrinsic plasma broadening which may be a simple or convoluted function depending on the broadening mechanisms Doppler, Stark, Zeeman, mass motion etc.

In optically thin conditions, i.e. $\tau(\nu) << 1$, the emission intensity $I(\nu) = S(\nu)\tau(\nu) = \varepsilon(\nu) D$. In the opposite limit of large optical opacity, $\tau(\nu) >> 1$, then $I(\nu) \simeq S(\nu)$. In a homogeneous collisional plasma with large optical depth, the radiation field may become strongly coupled to the local particle motion and in such (rare!) cases of thermodynamic equilibrium $S(\nu)$ is given by the Planck function.

The emission intensity will remain at the 'saturated' $S(\nu_o)$ level characteristic of the central frequency ν_o throughout the frequency profile, until, sufficiently far from the line centre $\tau(\nu)$ falls to unity, Fig.7. Corresponding to this frequency ν_1, the photons can escape with a mean free path $L = [a(\nu_1)]^{-1}$. At the frequency ν_1,

$$\int \rho . dr = \int N_z . dx = \frac{4\pi}{L(\nu) h\nu_1 B_{\ell,u}} \qquad (10)$$

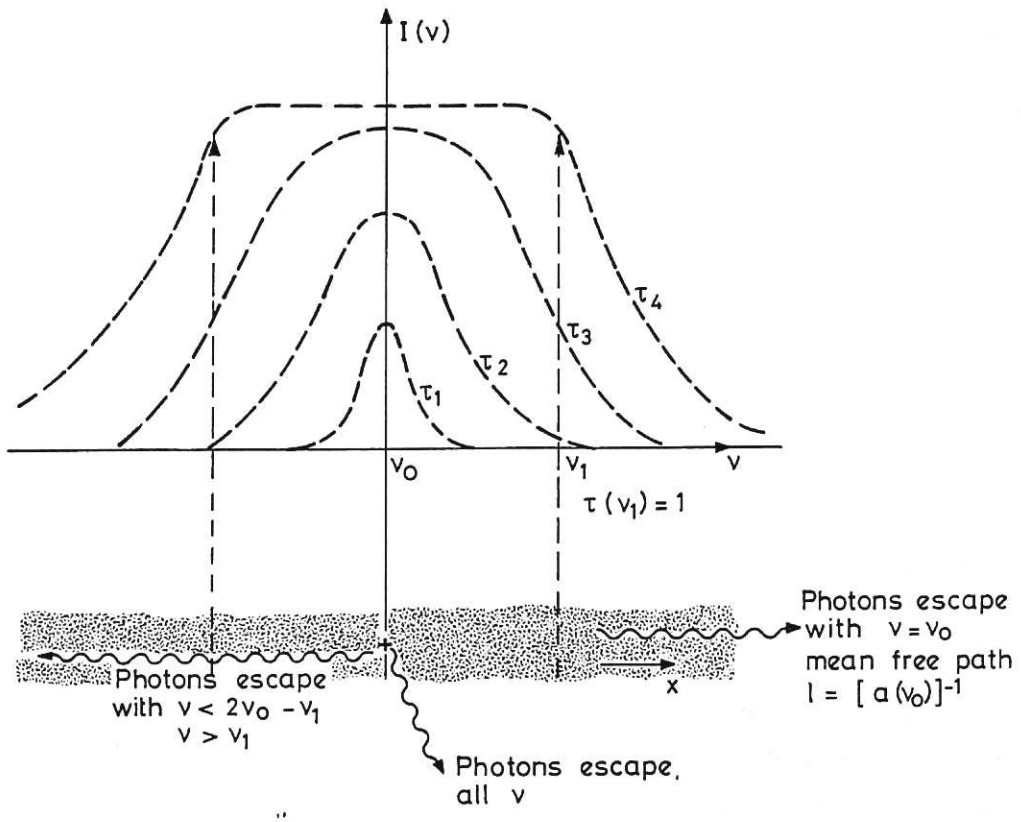

FIG.7 Emergent line profiles with various optical depths $\tau_1(\nu_o) << 1 << \tau_4(\nu_o)$, *the optical depth* $\tau(\nu)$ *depends on frequency* ν *and on its propagation depth through the homogeneous slab plasma.*

Expressed in gcm^{-2}, eq(10) becomes,

$$\int \rho . dr = \tau_o \Delta\nu_{\frac{1}{2}} \left(\frac{m\ M(z)\ c}{\pi e^2 f} \right) \frac{\sum_{z'}^{z''} N(Z)}{N(Z)} \qquad (11)$$

where $\Delta\nu_{\frac{1}{2}}$(Hz) is the 'intrinsic' full half-intensity width of the line and the factor $\frac{\sum_{z'}^{z''} N(Z)}{N(Z)}$ is a multiplier taking into account the population of the ionic species under consideration relative to the total ionic concentration.

In most laser-produced plasmas there are strong local spatial variations in the parameters and in the thermodynamic state. The intensity profile, even if flat-topped in the centre can depart markedly from a Planck function and will depend on the integrated effect of the non-stationary populations of the upper and lower levels throughout the plasma. In both plane-target and multi-beam compression experiments it is common to find that the first member of the resonance series of the dominant ion species

has an optical depth $\tau_o \sim 10 \rightarrow 100$, the second member with $\tau_o \sim 1$ and the higher members of the series with $\tau_o < 1$. The analyses of the emergent line shapes in terms of $L(\nu)$ and $\tau(\nu)$ is an important exercise in determining density, ρ and the parameter $\int \rho . dr$ in laser compression experiments, Section 3.3. The higher series members, being optically thin, are most applicable to the derivation of density from the Stark line shapes $L(\nu)$, while the optically thick lower members of the series are used to derive $\int \rho . dr$.

Model calculations, Irons (1980), of the optically thick emergent line profiles from streaming plasmas with radial temperature gradients has been performed for plasma conditions which obtain in plane-target irradiation experiments. These radiation transfer calculations, illustrated in Fig.8, can qualitatively at least account for the prominent self-reversal of the line core which is progressively blue-shifted with increasing distance from the target surface, Peacock (1977). Similar radiation transport model calculations have been successfully used by Malvezzi et al (1979), Tallents (1980) to account for the detailed shapes of the CVI Lyman series in plane target irradiation experiments. In hollow, conical target irradiation experiments where the streaming velocity

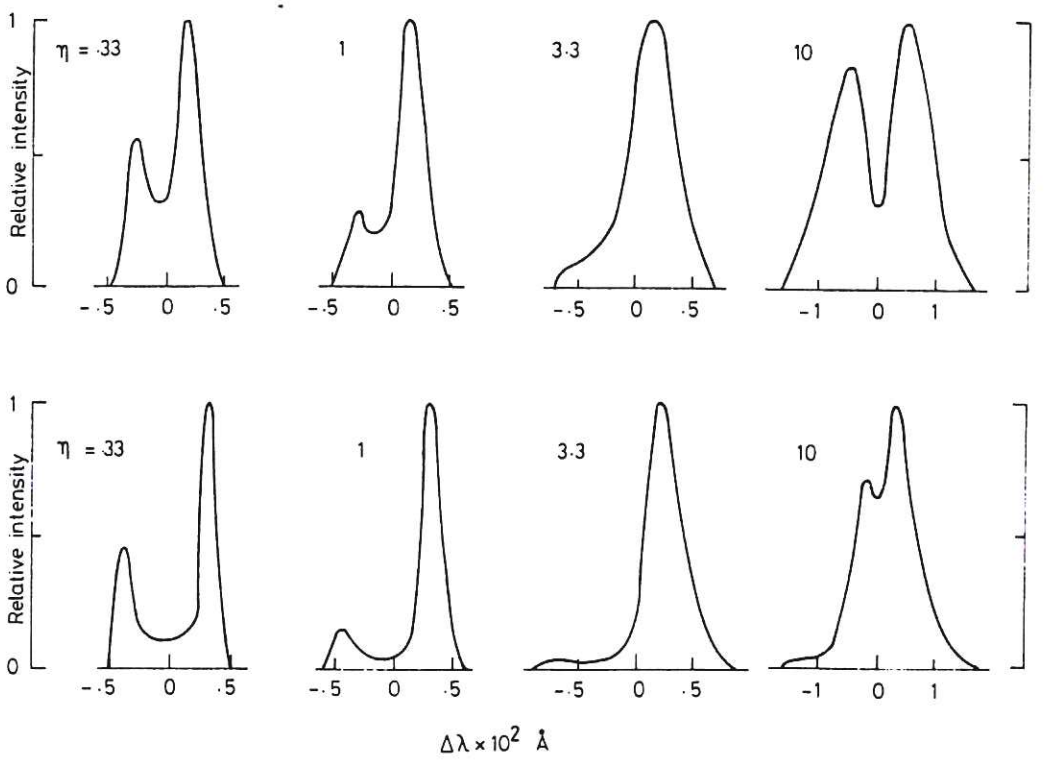

FIG.8 Line profiles of MgXI $1s^2\ ^1S_o - 1s2p\ ^1P_1$ from a Mg plasma, computed as a function of optical depth at line centre. Upper profiles have τ_o=10 while for lower profiles τ_o=100. The parameter η is the ratio of the mean expansion velocity to the HWHM of the thermal velocity spread. Each profile is normalised to unit peak intensity. IRONS (1980).

transverse to the conical axis is relatively low due to plasma thermalisation, the calculations, Fig.8, predict the appearance of an almost isolated blue wing component (see Fig.8, $\eta = 1.0$, $\tau_o = 10^2$) which may be mistaken for a Baranger-Mozer satellite to the forbidden 1s2s S_1 decay in He-like ions, Boiko, Krokhin et al (1974).

The effect of temperature gradients on the analyses of optically thick lines emitted from the core plasma in compression experiments has been considered by Skupsky (1978).

3.2 K_α Emission in Laser Produced Plasmas

At high laser irradiance, $\Phi_o \geq 10^{14}$ W cm^{-2} for 1μm wavelength, K_α emission is a feature of the X-ray spectrum as indicated in Fig.5. These screened transitions are of interest as indicators of the 'hot' electron energy deposition in regions of the target remote from the critical density layer where the supra-thermal electrons are generated. The 'hot' electrons are responsible for the high energy component of the X-ray continuum, Fig.6, and with an associated temperature $T_{eh} \gtrsim 10$ keV, their range in the solid target is typically tens of microns. For $\Phi_o \lambda^2 > 10^{15}$ W cm^{-2} x μm² hot electrons in fact become the dominant energy transport process in so-called 'explosive-pusher' compression experiments.

The bulk of the energy deposited from the hot electrons goes into heating and ionising the solid target, while only a relatively small fraction, $\sim$ 1% typically, results in K-shell ionisation of the cold material. Since a range of ion species results from the electron transport the K-shell emission is a distributed spectral feature, see Fig.5, composed of several separate lines extending from the fully screened $K_{\alpha_1\alpha_2}$ line (in neutral atoms or weakly ionised M-shell ions), partially-screened transitions in L-shell ions e.g. $1s^2 2s^n 2\ell^{n'} - 1s2s^n 2\ell^{n'+1}$, and unscreened valency electron emission e.g. Ly-α, from K-shell ions. The fully screened $K_{\alpha_1\alpha_2}$ transition can be thought of as having an unshifted position relative to the other K-shell lines which are progressively shifted to the blue as the ion charge increases. The intensity of the longest wavelength $K_{\alpha_1\alpha_2}$ line will reach a saturation level at an electron energy deposition rate which is sufficiently high to ionise all the M-shell electrons. Figure 9 shows the saturated intensity of Ca, $K_{\alpha_1\alpha_2}$ from an irradiated microballoon target coated with CaF_2. It is only this shaded feature of the total K-shell emission which

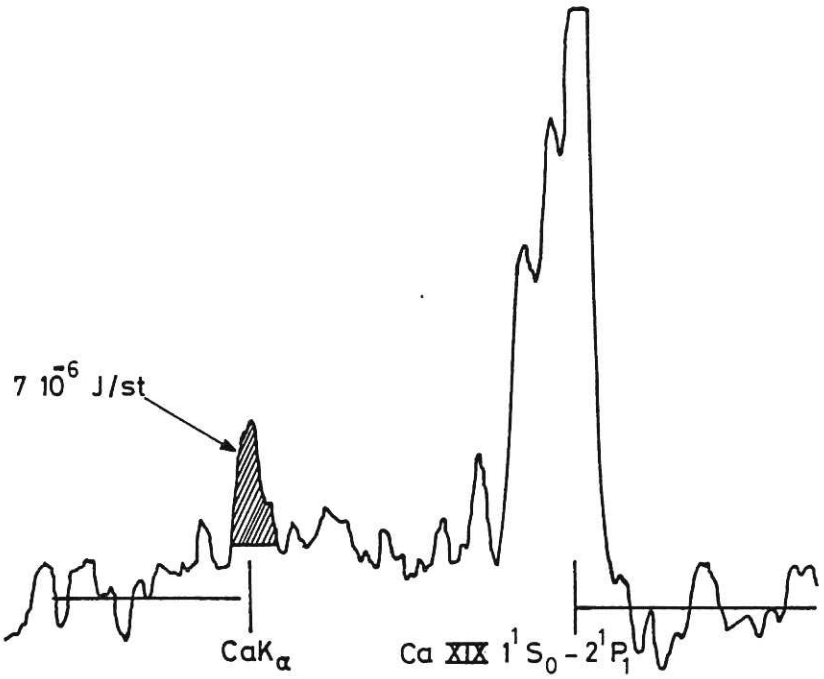

FIG.9 K-shell line emission from Ca ions produced by Nd-laser irradiation (30J in 0.1ns) of a CaF_2 coated glass microballoon. HARES et al (1979).

can be used as an electron pre-heat indicator. In order to measure the depth of hot electron penetration multi-layered targets have been used, see Hares, Kilkenny et al (1979), the characteristic K_α emission from each layer acting as a fluor tracer.

The X-ray continuum from the ablation surface can also give rise to K_α emission by photoionisation, this process being particularly efficient for photon energies just greater than the K-shell ionisation potential. The pertinent problem is to quantify the processes responsible for the intensity of the characteristic lines. In order to minimise photoionisation relative to electron excitation of K_α, the atomic number of the fluor is chosen such that $kT_e << E_{K_\alpha} < kT_{eh}$, where the thermal and hot electron temperatures occur on the LHS and RHS respectively of the inequality and E_{K_α} is the K-shell ionisation potential. Typically $kT_{eh} \geq 10keV$ and $kT_e \sim 0.1 \rightarrow 0.5keV$: Z = 20 is therefore a reasonable atomic number for the fluor. In irradiation experiments on multi-layered targets, Hares, Kilkenny et al (1979) have measured the fast electron deposition rate from the absolute K_α flux from a Ca fluor deposited on the reverse surface to that which was irradiated. Taking into account the saturation level of the unshifted K_α feature Hares, Kilkenny et al (1979) were able to deduce the current density, $\sim 10^{10} A\ cm^{-2}$, and the range and corresponding energy

$\sim$ 10keV, of the fast electrons. With an irradiation pulse of 20J in 100ps focused to an intensity of $\gtrsim 10^{15}$ W cm^{-2}, about 2J of energy is carried by these fast electrons.

In recent plane, layered target experiments these same authors have shown the effect of resistive inhibition of the electron currents by introducing an absorber, e.g. Au, with a variable density in front of the fluor. The line-integrated mass r_a (gm cm^{-2}) required to stop the electrons in the absence of inhibiting magnetic or electric fields will be constant irrespective of the local absorber density (gm cm^{-3}) and will depend only on T_{eh}. However, the electrostatic potential set up by the fast electron current is

$$V_R = \eta j_{he}^2 r_a/\rho \qquad (12)$$

and the use of sufficiently low ρ in eq(12) has the effect of inhibiting the cold electron return flow. As illustrated in Fig.10, reducing the

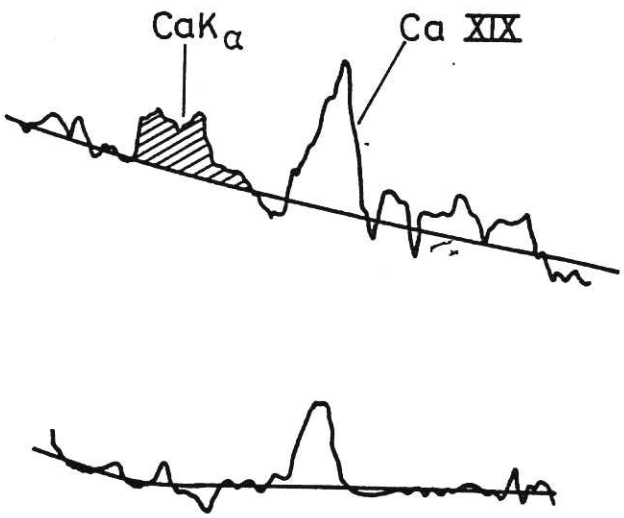

FIG.10 Emission spectrum from the Ca fluor in a laser irradiated plane layered target. The target layers are 0.1μm Al: 2.5μm Mylar: 3μm KCl: Au: 2μm CaF_2. The Al front surface is irradiated by a neodymium laser with an intensity on the Al surface of 3 x 10^{15}W cm^{-2}. Both spectra result from the same target and irradiation conditions but in the lower, the Au density is reduced to 0.62% of solid. The area mass density of the Au layer, 0.72mg/cm^2, is the same in both cases. BOND et al (1980).

density of the Au absorber by 0.6 reduces the K_α intensity by a factor of $\gtrsim$ 3. These experiments, Bond, Hares and Kilkenny (1980), demonstrate a potentially important technique for reducing fast electron preheat in laser compression experiments.

3.3 Line Profile Analysis

The use of collision-broadened emission line widths to derive the density in plane target interaction experiments dates back over a decade. Burgess et al (1967), for example, used simple estimates of the (electron-impact) half-widths of lines in the grazing-incidence region from alkali-like ions, e.g. OVI and KIX to give values of the electron densities which

were self-consistent to within a factor of two. Hydrogenic ions, being subjected to first order Stark broadening, are more powerful indicators of density and half-width estimates of the high quantum transitions of CVI have been used by Irons (1973) to measure $n_e < 3 \times 10^{18}$ cm^{-3} in the "spill-off" plasma from the irradiated surface.

Full profile fits of the Stark-broadened CVI Lyman series have been made by Galanti et al (1974) to measure the density profile in the ablation layer. It appears that at densities $n_e \simeq 10^{21}$cm^{-3} only a limited few of the transitions are free of opacity and line merging. In these full profile calculations referred to by Lee (1979, I, II, III), Lee (1979) and Lee et al (1979) as 'standard profiles' the ion microfield due to the main perturbers C^{5+} and C^{6+} has been calculated using Hooper's formalism, O'Brien and Hooper (1972), Tighe and Hooper (1978), and is corrected for the screening effect of the electrons. Electron collisions, responsible for broadening the core of the lines, is taken into account in the impact approximation. Smith and Peacock (1978) overcome the line centre radiative-transfer problem and much of the complications at high density by fitting a relatively simple Holtsmark profile, modified to take into account correlations and screening, to the optically-thin far wings only, Fig.11. In this region of the line profile electron impacts and instrumental effects

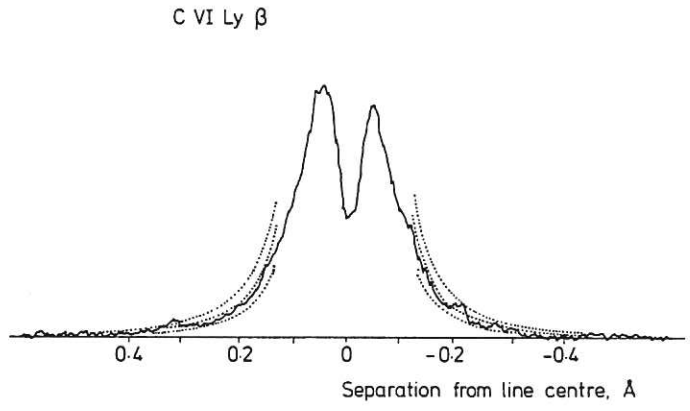

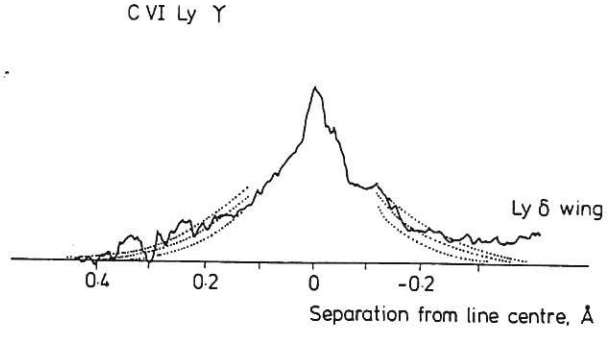

FIG.11 Profiles of CVI Lyman lines emitted from the critical density region of the plasma formed at the surface of a Nd-laser irradiated $(CH_2)_n$ target. Theoretical predictions .... of the line wing intensity are shown for several values of electron density from $n_e = 1.4 \times 10^{21}$ cm^{-3} (lowest), through 1.8×10^{21}cm^{-3} to 2.5×10^{21}cm^{-3}. SMITH and PEACOCK (1978).

represent an insignificant modification to the intensity. The adjacent free-bound continuum in LTE with the upper level of the emitted line, is used as an absolute intensity reference for the line wing intensity. Accuracies of $\sim \pm 20\%$ in the density are suggested for the peak density $\simeq 2 \times 10^{21}\ cm^{-3}$ in these plane target experiments.

In symmetrical irradiation experiments on microballoon targets, where plasma is compressed by spherical convergence to densities several orders of magnitude higher than can be obtained with single-beam, plane-target irradiation, Yaakobi et al (1977) have employed, with some success, Stark-broadened H-like ions of rare gases as density monitors. These authors use the optically thick Lyman lines to derive $\int \rho . dr$ and the higher series members, which are optically thin, to derive density.

In these and similar laser compression experiments the Lyman lines of the elements of interest lie in the X-ray region and crystal dispersion of the spectrum is necessary. Space resolution of the emission is effected by a slit aperture between the plasma source and the (plane) crystal, yielding an intensity pattern as illustrated in Fig.12. With a sufficiently narrow slit the spectrum from the ablated surface of the microballoon is readily differentiated from that in the implosion core. An example of the

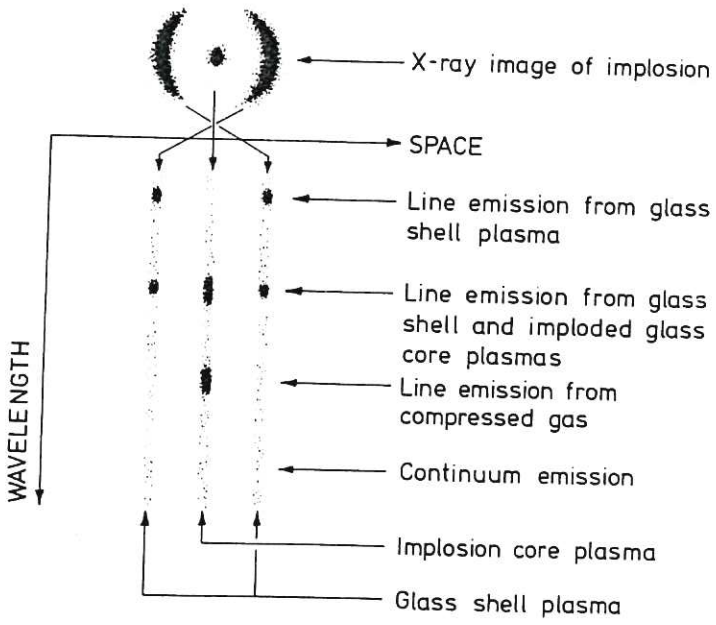

SCHEMATIC OF SPACE RESOLVED SPECTRUM

FIG.12 The X-ray image of a 2-beam irradiated spherical target space-resolved and dispersed by a minature slit aperture of plane crystal spectrometer.

spectrum from such an instrument is shown in Fig.13. The higher density in the core is typified by a relatively intense continuum overlayed by Stark broadened resonance lines of neon (from the gas fill) and the H- and

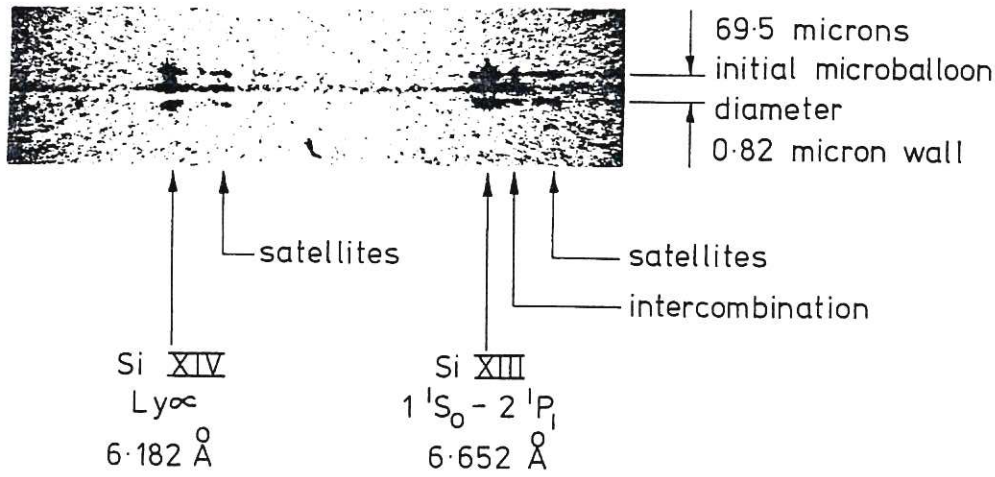

FIG.13 Space resolved X-ray spectrum from a laser-irradiated glass microballoon filled with neon to a pressure of 8.5 bar. After EVANS et al (1978).

He-like resonance lines of Si from the glass shell, the latter being considerably broader in the core than at the ablation surface. Since these first 'exploding-pusher' experiments' for which values of $\int \rho dr$ ($\sim 10^{-4}$ gm cm^{-2}) and ρ ($\sim$ 0.2gm cm^{-3}) were typical e.g. Yaakobi et al (1977), it has become apparent that there is some difficulty in achieving a consistent set of plasma parameters which will account for the observed profiles of <u>all</u> of the transitions, both those that are optically thick and also the optically thin. In part, the difficulty is due to measurement of only the gross widths of the lines which are not a unique function of the two major variables, n_e and τ_z. A detailed comparison of the theoretical line shape over an extended wavelength region <u>is</u> a unique function of n_e and τ_z and of the spatial variation of those parameters as inserted in the radiation transport model. Unfortunately, however, the coarse features such as half widths are often the only experimental observables. Kilkenny and Lee et al (1979) have considered this problem of data reduction and plot the results of a 'best-fit' to the theoretical profiles on a n_e, N(Z), (equivalent to n_e, τ_z) diagram for all the lines as in Fig.14. The region of n_e, N(Z) parameter space where there is consistency (n_e = 1.5 x 10^{23}cm^{-3}, N(Si^{+13})= 10^{21}cm^{-3}) defines the core parameters in this Ar-filled micro-balloon compression experiment, Kilkenny and Lee et al (1979). The annotation

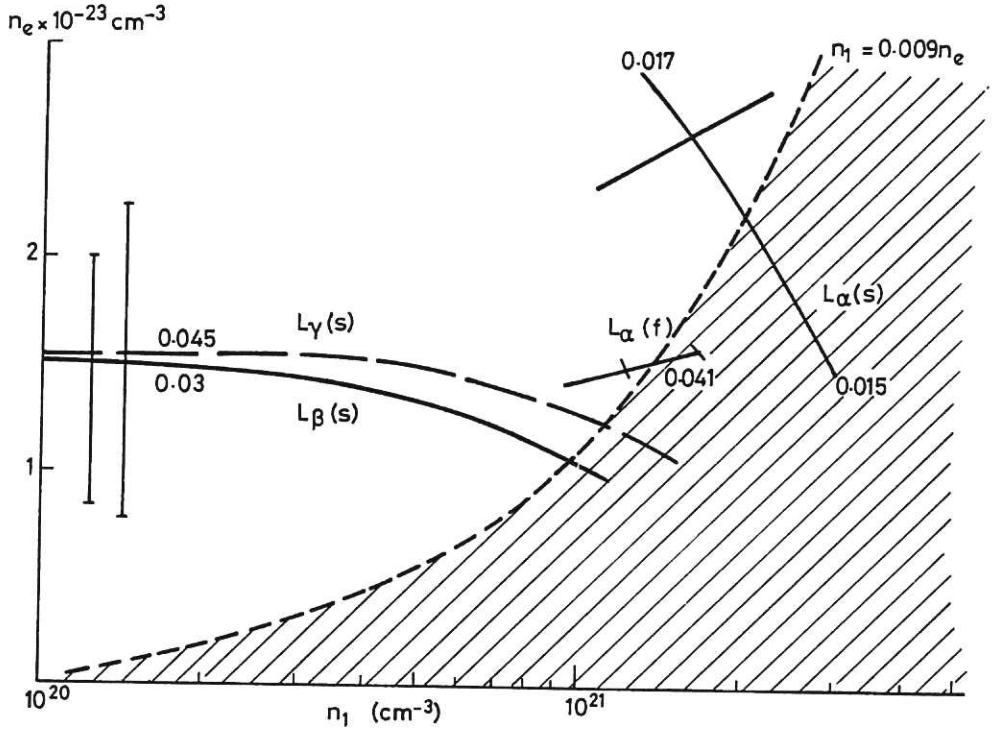

FIG.14 Indicator plots of the Si XIV Lyman line profile data derived from the core X-ray emission in an Ar-filled microballoon irradiation experiment. Each plot in the parameter space, defined by the electron (perturber) density and the emitter ($n_1 \equiv N(Si\ XIV)$) density corresponds to a separate line of the Lyman serices. From the ratio of the Si XIII/ Si XIV recombination continua intensities it is concluded that $n_1 \leq 0.009\ n_e$, thus excluding the shaded region as a possible region of fit. There is apparently a region of best fit for all three lines around $n_e = 1.5 \times 10^{23}$ cm^{-3} and $n_1 = 10^{21}$ cm^{-3}. The 'full' line broadening theory "f" due to LEE (1979) gives a more consistent fit to the broadening of all the series members than is the case using the 'standard' "S" theory. The numbers associated with each indicator plot refer to the quality of the experimental profile fit to the theory. KILKENNY et al (1979).

"S" refers to the 'standard' computations of the Stark profiles including quasi-static ion broadening, corrected for multiple ion species perturbers, Debye screening, correlations, and electron impact effects. The annotation "f" refers to more sophisticated calculations by Lee (1979 I, II, III) which are discussed in Section 5 and include ion dynamics, polarisation and fine-structure effects. The inclusion of the "f" profiles, Fig.14 gives a more convincing consistency to the analyses.

Even higher densities have been reported in recent laser irradiation experiments, e.g. Auerbach et al (1980), Yaakobi , Skupsky et al (1980) the compression takes place not by explosive deposition of the fast electrons in the inner surface of the shell but by relatively shock-free ablation of thick $\gtrsim$ 5μm, walled targets with high Z, e.g. Ar gas filling. Radiation cooling by the argon assists in the convergence to a compressed

plasma density of 1 → 6 gm cm^{-3} and $n_e \simeq 1.5 \times 10^{24} cm^{-3}$, but with a somewhat reduced temperature $T_e < 1$ keV. Figure 15 illustrates a profile analysis of the Ar, Ly-β line in such an experiment.

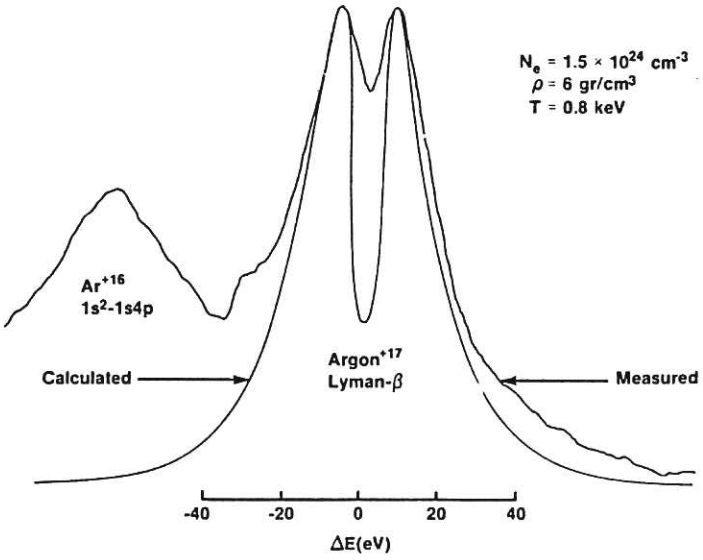

FIG.15 Ar lines from core plasma produced by symmetrical irradiation of plastic coated glass shell filled with ∿ 10 atmospheres Argon. $1s^2$-1s4p transition broadening is comparable to that of Ly-β due to cross over from quadratic to linear Stark effect at $Ne = 1.5 \times 10^{24} cm^{-3}$. Calculated Stark profile does not take into account ion dynamics or opacity. The inclusion of the latter (estimated value of $\tau_o \simeq 0.5$) improves the profile fit. YAAKOBI et al (1980).

4. ABSORPTION SPECTROSCOPY

Absorption spectroscopy has been adapted to the study of laser-driven microballoon implosions by Key, Lewis et al (1978). The technique has proved particularly useful for 'explosive' compression studies of high pressure (∿ 100 bar) gas-filled microballoons and in 'ablative' compression experiments, where relatively low temperature ($T_e \lesssim 100$ eV) and relatively high density ($n_e \gtrsim 10^{23} cm^{-3}$ and corresponding material density of several gm cm^{-3}) have been achieved. It is necessary that the backlighting continuum source, usually produced by laser irradiation of a subsidiary high Z target, has a higher brightness than the probed plasma at the frequency of interest. The optical depth, associated with free-bound absorption $a(\nu)$ in the probed plasma, is derived from the experimental variation of the probe light transmission $T(x,\nu)$, viz,

$$\int a(\nu)_{q\nu} dx = \tau(x) = \ell n \left| \int I(\nu) T(x,\nu) d\nu \Big/ \int I(\nu) . d\nu \right| \qquad (13)$$

In order to analyse the results in terms of $\int \rho . dr$ the concentration of ionic absorbers in the probed plasma and the plasma dimensions are required.

An example of time-resolved shadowgraphy of a polymer-coated microballoon is shown in Fig.16. Transmission cut-off of the probe light at a frequency ν, corresponding to $h\nu \simeq 2$keV, occurs initially at the walls of the target, Fig.16, and converges towards the core as the implosion proceeds. It is often useful to delay the back-lighting pulse until after the start of the implosion in which case the streak record shows the earlier emission from the irradiated walls as well as the 'absorption' sequence illustrated in Fig.16.

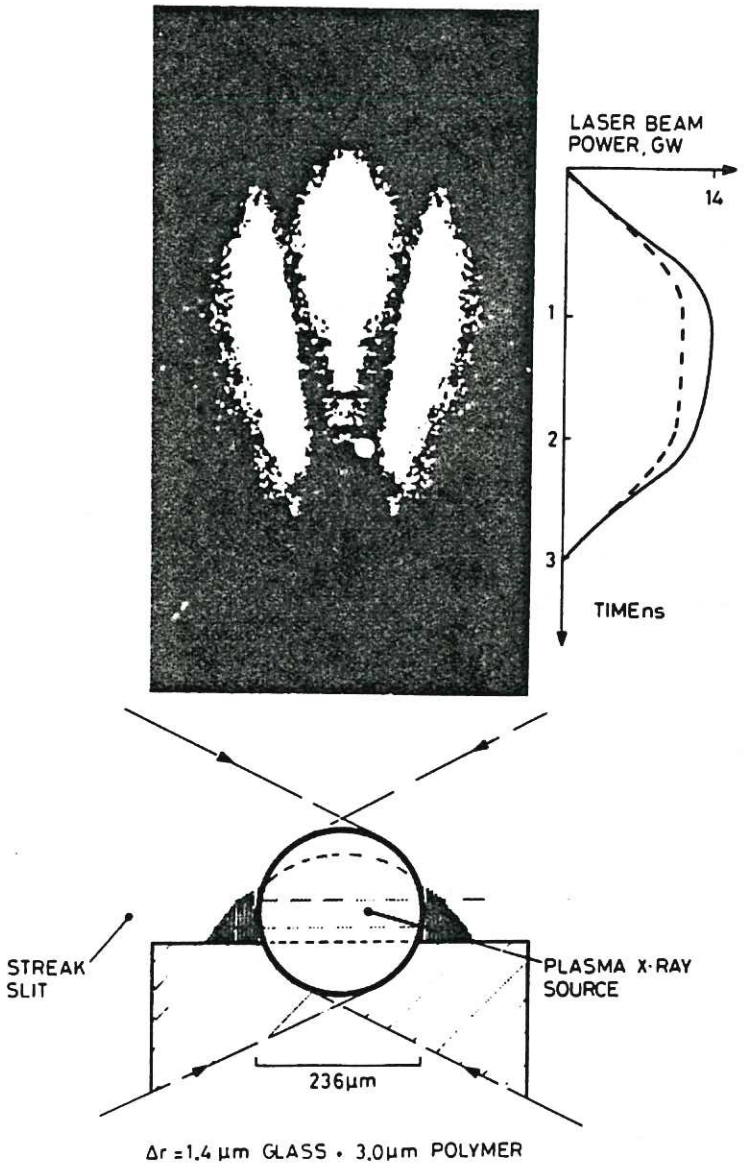

FIG.16 X-ray shadowgraphy using an image intensifier camera with a CsI coated photo cathode. The picture shows absorption of the backlighting X-rays ($h\nu \leq 2$ keV) due to the dense plasma from the microballoon wall. Convergence with time of the zones of maximum absorption indicates the progress of the implosion. In this ablative compression experiment the glass microballoon is overcoated with a 3μm ablative layer of polymer. Rutherford Laboratory, (Science Research Council) Annual Report of the Laser Division, RL-79-036 (1979).

An interesting variation of absorption spectroscopy has been applied to the spectrum from the outer shell region in ablatively-driven experiments when there is relatively low specific energy deposition ∿0.2J/ngm. The spectrum shows absorption features in the light emitted from the core plasma, Yaakobi McCrory et al (1980). Analyses of the resonance line absorption of the $1s^2$-1s2p, 3p transitions in Si^{+12} and their satellites of Si^{+11}, Si^{+10}, etc., indicate that $\int\rho.dr$ in the outer shell plasma is $\sim 0.6 \times 10^{-3}$ g/cm² with an electron density $n_e \sim 10^{23}$ cm^{-3} and a temperature (derived from Saha ionisation balance) of $T_e \sim$ 150-200 eV. These values are in contrast to the core parameters of $T_e \sim 600$ eV and $n_e \sim 5 \times 10^{23}$ cm^{-3}.

It is of interest that the intensity reversal of the 1s3p radiation is asymmetrically biased towards the red wing of the emission line from the core. This is due to a quadratic Stark shift of the 1s3p level, Section 6, which displaces the line to higher photon energy at the higher density in the core plasma.

5. EXPERIMENTAL TECHNIQUES

Within the last decade there has been a quite remarkable development of diagnostic techniques aimed at the study of laser-produced plasmas on a timescale of picoseconds and with a spatial resolution in the order of microns. Many of the developments are described in articles by the Lawrence Livermore group e.g. Attwood (1978), Coleman (1978), Ahlstrom et al (1978), Attwood, Ceglio et al (1979) and are surveyed by Peacock (1979). A wide range of physical principles is involved encompassing such disparate topics as radiation chemistry of test materials exposed to the fusion micro-explosion and X-ray absorption spectroscopy. While in Sections 3 and 4, we have touched on the importance of emission and absorption spectroscopy in this section we illustrate the progress in diagnostic methods by highlighting just two of the more important technological developments, namely apparatus for time resolution and for imaging the x-ray emission.

Temporal resolution of the X-ray emission from the plasma is effected by projecting its image onto a photocathode of a gated image intensifier. These electron intensifier tubes, using proximity acceleration grids and electronically swept electron beams, have an inherent resolution of ∿ 1ps and 20ℓ/mm. For X-rays in the energy range hν ∿ 1→10keV, the photocathodes are typically a 200Å thick coating of Au on a Be substrate.

A spongy coating of CsI of thickness 20→200μm, depending on the X-ray energy, can increase the overall sensitivity of the X-ray camera by a factor of ∿ 20. Since one dimension of the image plane is reserved for the time sweep only a thin slice of the geometrical image of the plasma is displayed as in the shadowgraphy of a microballoon implosion illustrated in Fig.16.

The X-ray streak camera may also be used to time-resolve the X-ray spectrum dispersed via a Bragg crystal as in Fig.17. This streak record of an irradiated glass microballoon with a neon gas filling indicates that sufficient spectral resolution, ∿ 5 mÅ, at 6Å with a PET crystal, is retained with this system to measure the Stark widths, (∿ 180mÅ for Ly-β NeX) of the line emission from the compressed core plasma. The Na ion lines from the irradiated glass shell are less broadened and extend over a longer period of time, Key, Lewis, Lunney et al (1980). The timescales

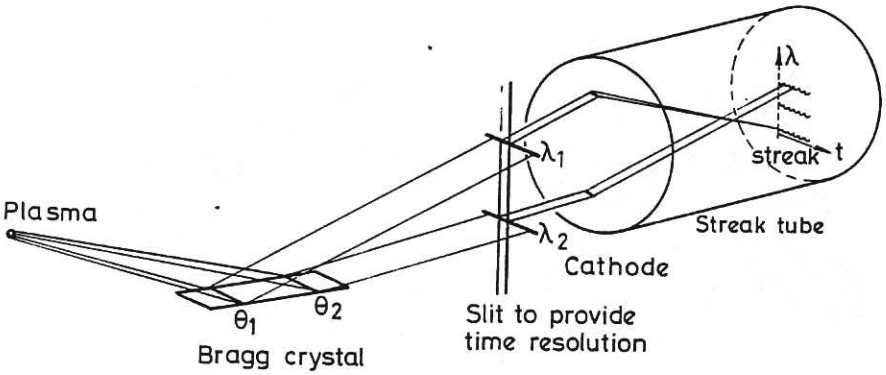

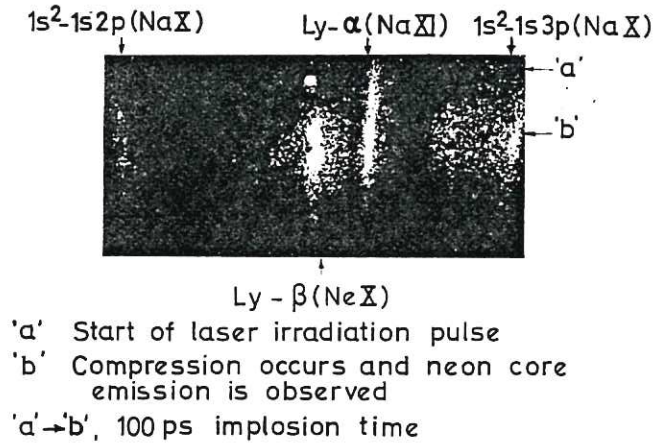

'a' Start of laser irradiation pulse
'b' Compression occurs and neon core emission is observed
'a'→'b', 100 ps implosion time

FIG.17 Apparatus for X-ray streak spectroscopy showing part of the time-resolved X-ray spectrum (time resolution ∿ 70ps and spectral resolution λ/Δλ ∿ 500) from a laser irradiated glass microballoon. KEY, LEWIS et al (1980).

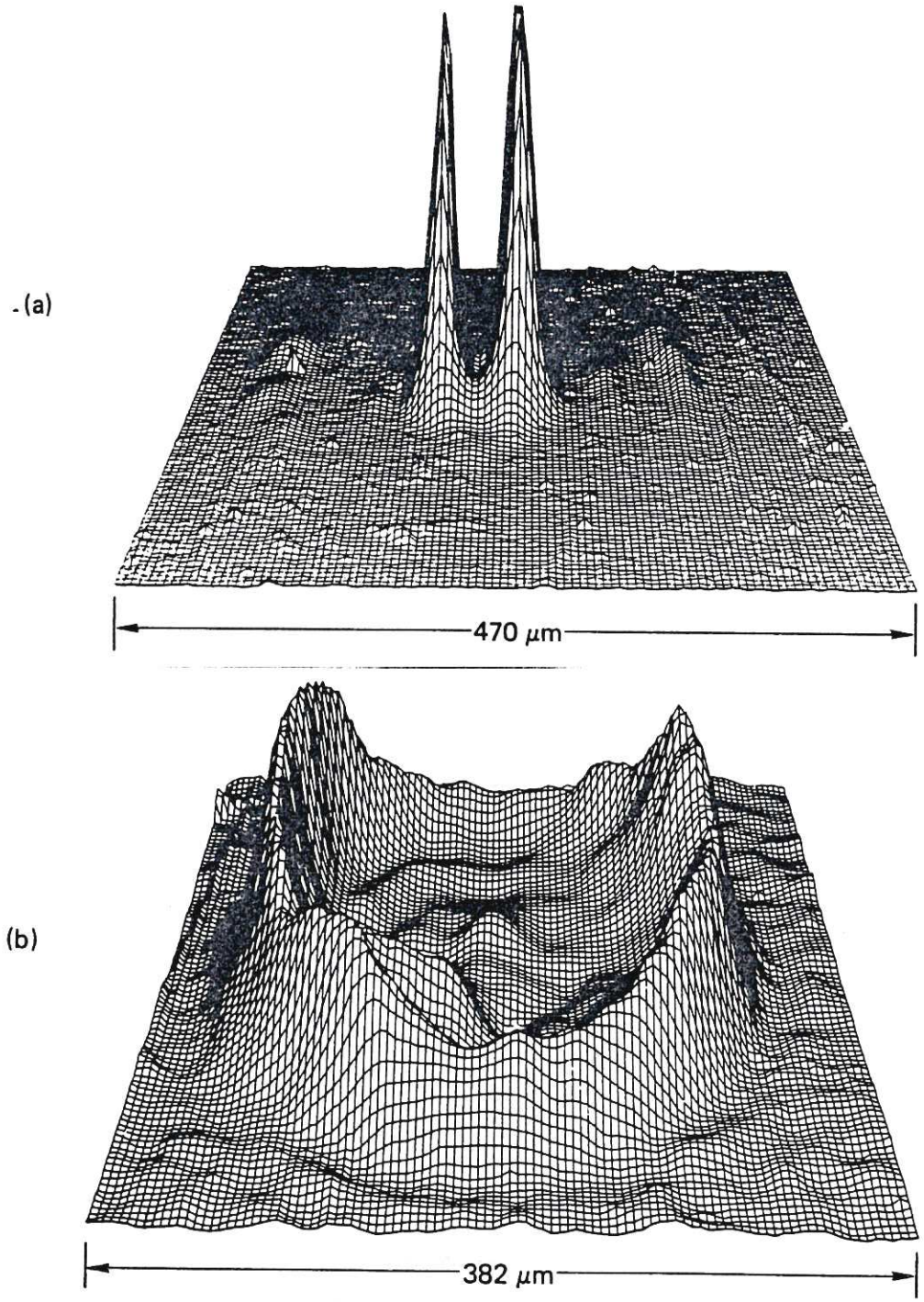

FIG. 18 Coded aperture image of X-ray emission from laser irradiated glass microshell targets with 2mg/cm³ DT gas fill. (a) Thermal emission in the spectral window 4-7 keV is dominated by two disc-shaped regions of glass plasma (separated by expressed DT fuel). (b) Supra-thermal X-ray image in spectral window 17-30 keV has a hollow shell structure whose diameter is approximately that of the original microballoon. CEGLIO and LARSEN (1980).

of the separate emission lines have recently been exploited in measurements of the mass ablation rates from irradiated multi-layer targets. The layers are of dissimilar elements each layer emitting its own characteristic X-ray 'signature', Key, Evans et al (1980): Lewis, Lamb et al (1980).

Two quite different approaches to X-ray imaging have been used in the study of laser irradiated targets. Reflection microscopy is perhaps the obvious technique and has the advantage of good resolution $\sim$ 1μm and relatively long objective distances which allows the image-forming components to remain undamaged during a micro-explosion. A less obvious and very effective technique, developed by Ceglio and his co-workers at the Lawrence Livermore Laboratory, is that of coded-aperture-imaging, giving a capability for 3-D analysis on reconstruction of the image: Ceglio and Smith (1978), Ceglio, Attwood and George (1977), Ceglio, Shavers et al (1979). The coded apertures used are typically free-standing micro Fresnel zone plates 5→25μm thick with zone numbers $100 \leq N \leq 250$, the width of the outermost zone Δ_r = a few microns, this being the same order as the planar resolution. Tomographic (in depth) resolution of a few 10's of microns is achieved. The coded aperture technique is not only a powerful method for X-ray imaging but it has also been adapted for measurements of the spatial emission of the fusion reaction products from laser-irradiated, D-T filled microballoon targets, Ceglio and Coleman (1977).

The X-ray light in different spectral regions can be isolated using appropriate filters in front of the coded shadowgrams of the source. Figure 18 indicates the distinctive differences in the thermal (4→7keV) emission from the compressed core and the (17→30keV) emission which originates from local energy deposition in the shell plasma of the supra-thermal electrons generated at the critical density surface, Ceglio and Larsen (1980).

6. ATOMIC PHYSICS OF DENSE PLASMAS

In the spectroscopy of 'ordinary' plasmas the energy distribution of the electrons and of the upper bound atomic levels collisionally-coupled to the free electron states are described by Boltzmann statistics. Binary collision processes are the rule and the impact approximation, Griem (1974), in which the duration of the collision is much exceeded by the time between collisions, gives a reasonable basis for line broadening calculations. Collective particle motion involves many particles within the Debye sphere whose characteristic dimension is $\lambda_D = v_{th}/(\sqrt{2}\omega_{pe})$, and leads generally to only weak perturbations to the energy level shifts. Modifications to these theoretical treatments to account for the emission spectra from ultra-dense plasma conditions such as obtained in laser-irradiation experiments on solids have been discussed by Vinogradov, Sobelman and Yukov (1974), Peacock (1978) and by Burgess (1978). Atomic collision rates, energy levels, and emission line shapes can all be

affected. Corrections to these quantities are due to the short inter-particle separations, which can be of the order of the atomic structure dimension, and to the short collision mean free paths, which may be of the order of the emission wavelength. Modifications to the plasma micro-fields to take into account strong collective particle motion, ion microfield screening and ion dynamics are required for a complete description of Stark broadening. These effects become all the more pronounced when dealing with highly charged ions and at the highest densities reached in laser-irradiated experiments.

For the most part, radiative transition probabilities remain unchanged in high density plasmas. There are exceptions as when parity mixing of doubly excited states is induced by the strong plasma microfields, as discussed by Davis and Jacobs (1975). The oscillator strength involved in photo-ionisation cross-sections may also be altered, Rozsnyai (1976). Again, the binary approximation to collision rates will remain valid to very high densities, $n_e \gtrsim 10^{25} cm^{-3}$ for the resonance lines of NeX, as discussed by Burgess (1978). It is a matter of some conjecture, however, to what extent long range interactions will be affected by Debye screening and particle correlations so as to alter the near-threshold collision cross-section. One might expect this to occur when the electron-emitter correlation length, λ_{ez}, is of the order of the Debye length i.e. when

$$\frac{Ze^2}{kT_e} \simeq \frac{v_{th}}{(\sqrt{2}\omega_{pe})} \qquad (14)$$

Electron-ion correlations would be expected to modify the electron velocity distribution when their correlation length is of the order of the electron separation, i.e. when $\lambda_{ez} \gtrsim r_{oe}$, or

$$\frac{Ze^2}{kT_e} \simeq \left(\frac{3}{4\pi n_e}\right)^{1/3} \qquad (15)$$

Of course, in extreme density plasmas when the electron separation is of the order of the de Broglie wavelength, $\lambda_B = (h^2/2mkT)^{1/2}$, i.e. as the plasma becomes electron degenerate, electrons will be removed from the free energy distribution and threshold excitation rates in particular will be affected.

In high density plasmas we might expect Debye screening (which occurs when the number of particles in a Debye sphere $n_D \to 1$ or less) to split

and shift the energy levels towards the ionisation limit. This lowering of the ionisation limit, assuming a Debye potential model, is $\Delta\psi \simeq e^2/\lambda_D$, and can be equated to the quantum level in the last bound state, 'n', which for hydrogen ions is given by

$$n_e(cm^{-3}) = 5 \times 10^{21}\, T_e(eV)\, Z^2 (1 + Z)^{-1} n^{-4} \qquad (16)$$

If the inter-particle distance, r_{oz}, becomes comparable to the dimensions of the quantised orbit, a condition readily reached even for low quantum states in laser compression experiments, then the idea of atomic structure loses significance. The effects, therefore, of Debye screening and ion correlations are to alter, albeit perhaps only slightly, the ionisation balance in the plasma.

In contrast to the foregoing, line profiles are relatively sensitive to changes in the basic statistical properties of the plasma when at high density the mean interaction energy becomes of the order of or exceeds kT_e. The physical processes which need to be incorporated in a full treatment of the theory of collision and Doppler broadening is discussed by Burgess (1978). Theories developed originally for use in modest density plasmas have been modified, e.g. Griem, Blaha and Kepple (1979) and have been used as we have seen (Yaakobï et al, 1977, 1979) with some success in laser-driven compression experiments. Consistent treatment of the shielding of the emitter perturber interaction, including electron-electron and electron-ion correlations, is possible in these calculations as long as both $r_{oe} < \lambda_D$ and the impact approximation holds. The effects of multi-component ion perturbers can also be treated following O'Brien and Hooper (1972) and Tighe and Hooper (1979).

The most important very recent developments in Stark broadening theory have concerned the separate but related effects of high density and high emitter charge. When the ion-ion correlation length, λ_{zz}, becomes of the order of the ion separation, a condition given by

$$Z^2 n_e = 1 \times 10^{20}\, T_e^{\,3} \qquad (17)$$

(n_e in cm^{-3}, T_e in eV) and for multiply ionised species at still higher density when $r_{oz} \sim \lambda_D$, then the local field seen by every ion is quite different from the average microfield. Screening of the bound electron from its parent

nucleus is predicted to cause (polarisation) shifts. For high Z emitters ion dynamics are considered to be important. Sophisticated calculations of collision broadening in multi-component plasmas by Lee (1979, I, II, III) and Lee et al (1979) which include electron-ion correlations to second order in RPA, fine structure splitting and ion dynamics, indicate that for high Z emitters, marked effects can occur both in line shifts and in asymmetries and that resonances due to sound waves can contribute to the line wings. Figure 19 indicates the predicted effect of the perturber charge on Ar Ly-γ at $n_e = 3 \times 10^{23}$ cm^{-3}. The predicted profile is largely independent of the perturber charge in the quasi-static approximation, whereas the inclusion of ion dynamics reveals a marked sensitivity to the exact charge on the perturbers, Lee and Freeman (1980).

Another predicted effect of high Z ions in laser produced plasmas is the suppression of Doppler broadening due to the short collision mean free path of the emitter ion. When this distance becomes of the same order as the emission wavelength the individual Doppler shifts are no longer incoherent and phase cancellation of the wave packets can, in theory result in line narrowing, Burgess, Everett and Lee (1979).

It is pertinent to ask whether any of these predicted high density effects have actually been observed? In some cases the answer has to be a qualified negative. Perhaps the reason is that the effects require finer scale resolution of the observables than has been achieved so far in laser compression experiments. There are, however, recent indications of the appropriateness of Lee's 'full' line profiles, in the experiments by Kilkenny et al (1979), Fig.14.

Also recent tentative evidence for Doppler narrowing has been reported in laser plasmas by Burgess, Everett and Peacock (1980). These authors study the n=2, Δn=0, transitions of VXIV $\rightarrow$ VXX which conveniently lie in a fairly narrow wavelength region between 120Å and 180Å. In plane target irradiation conditions the line profiles are calculated to be broadened mainly by Doppler effects and experimentally they appear to exhibit a charge-state dependent line narrowing.

A final consideration in our pursuit of the importance of the effects associated with high ion charge is the ultimate charge state which can be generated in laser irradiation experiments. With relatively long ($\sim$ few ns) laser pulses and surface light intensity $\geq 10^{15}$ W cm^{-2}, K-shell spectra of

elements up to atomic numbers Z ≈ 30 have been observed. In M-shell spectra, ions with charge states exceeding + 50 are readily obtained.

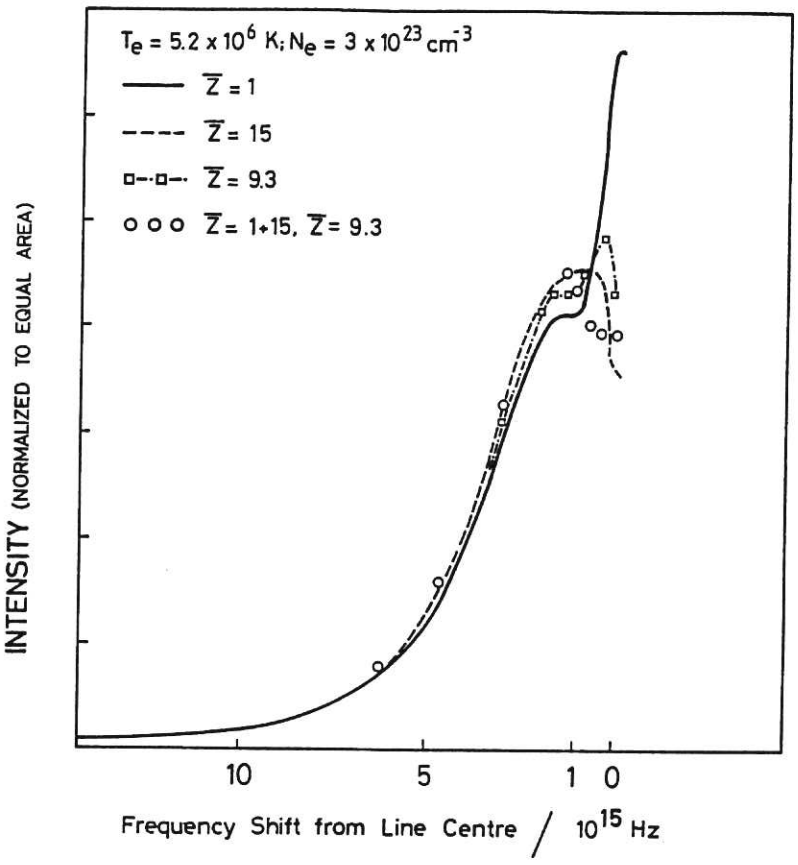

FIG.19 Computed line profiles of Ly-γ Ar XVIII including ion dynamics for various values of the mean charge state $\overline{Z}$ of the perturber ions. Increasing $\overline{Z}$ from 1 to 15 lowers the peak intensity by ∿ 40% and broadens the profile. The profiles □ – · □ – · and o o o o correspond to a mean $\overline{Z}$ of 9.3, the former being due to a fictitious single chemical species the latter due to a mixture of Z = 1 and Z = 15. Purely static ion model calculations show only a weak dependence on Z and give a central intensity which is a factor of ∿ 1.5 higher (with a consequently narrower profile) than the full curve corresponding to the dynamic calculations for Z = 1. LEE and FREEMAN (1980).

7. ACKNOWLEDGEMENTS

The author would like to acknowledge the help, in terms of advice and diagrams, generously given by scientists in the research programmes on laser interaction with matter. The author has leaned particularly on the work in the laser divisions of the Rutherford Laboratory and the Lawrence Livermore Laboratory.

REFERENCES

AHLSTROM H G, COLEMAN L W, RIENECKER Jnr. F, SLVINSKY V W, J Opt.Soc. Am, Vol 68, No.12, 1731-1741 (1978).

ATTWOOD D T, IEEE Jnl of Quantum Electronics, Vol. QE, 14 No.12 pp 909-923 (1978).

ATTWOOD D T, CEGLIO N M, CAMPBELL E M, LARSEN J T, MATHEWS D M and LANE S L, Lawrence Livermore Laboratory Preprint, UCRL-83541, (1979).

AUERBACH J M, MEAD W C, CAMPBELL E M et al, Phys.Rev.Letts. 44, No.25, 1672-1675 (1980).

BOIKO V A, KROKHIN O N, PIKUZ S A and FAENOV A Ya, Zh.E.T.F.Pis.Red 20 115-119: Trans. J.E.T.P.Lett. 20, No.2 50-51 (1974).

BOIKO V A, CHUGUNOV A Yu, FAENOV A Ya, PIKUZ S A, SKOBELEV I Yu, VINOGRADOV A V, YUKOV E A, J Phys B (Atom Molec.Phys) Vol 12, No.2 213-220, (1979).

BOIKO V A, PIKUZ S A and FAENOV A Ya, J Phys B (Atom Molec Phys) Vol 12, No.11 1889-1910 (1979).

BOND D J, HARES J D and KILKENNY J D, Phys Rev.Lett 45 No.4 252-255 (1980).

BRISTOW TC, CRAXTON R S, DeLETTREZ J et al, Proc. 8th Int. Conf. on Plasma Physics and Controlled Fusion Research, Brussels 1980 paper IAEA CN-38/B-4 to be published IAEA Vienna 1981.

BURGESS D D 1978(a) in "Physics of Ionised Gases", publ Institute of Physics, Belgrade, 543-577, also UKAEA Culham Laboratory Report CLM-P568.

BURGESS D D, EVERETT D and LEE R W, J Phys.B, 12, L755-758, (1979).

BURGESS D D, EVERETT D and PEACOCK N J, paper presented to 5th Int. Conf. on Spectral Line Shapes, Berlin 1980, see Proc. of Conf.

BURGESS D D, FAWCETT B C and PEACOCK N J, Proc. Phys.Soc. 92, part 3, 805-816, (1967).

CEGLIO N M, ATTWOOD D T and GEORGE E V, Jnl Appl Phys. 48 No.4. 1566-1569, (1977).

CEGLIO N M and COLEMAN L W, Phys.Rev.Letts, 39 20-24 (1977).

CEGLIO N M and LARSEN J T, Phys.Rev.Letts, 44 No.9 579-582 (1980).

CEGLIO N M, SHAVERS D C, FLANDERS D C and SMITH H I, Lawrence Livermore Laboratory Preprint UCRL-82684 (1979).

CEGLIO N M and SMITH H I, Rev.Sci.Instrum. 49 15-20 (1978).

CHRISTIANSEN J P, ASHBY D E T F and ROBERTS K V, Computer Physics Communications 7, 271-287, (1974).

COLEMAN W W, Proc. of Varenna Summer School on Plasma Physics - Diagnostic Techniques, Sept. 1978, Publ. by Pergamon Press 1979, 483-509.

COLOMBANT D and TONON G F, J Appl. Phys. 44, No.8, 3524-3537, (1973).

DAVIS J and JACOBS V L, Phys.Rev.A. 12 2019 (1975).

DAWSON J M, Phys. of Fluids 7 981 (1964)

DAWSON N M and OBERMAN C, Phys. of Fluids 5 No.5 517 (1962).

DONALDSON T P, Culham Laboratory Report CLM-R153 (1976).

DOSCHEK G A, FELDMAN U, DAVIS J and COWAN R D, Phys.Rev.A 12 980 (1975).

EVANS R G, KEY M H, NICHOLAS D J et al, Proc. 7th Int. Conf. on Plasma Physics and Controlled Fusion Research, Innsbruck, Austria, (1978). Publ. IAEA Vienna as Nuclear Fusion Supplement Vol III, pp 87-102 (1979).

GALANTI M and PEACOCK N J, J.Phys.B (Atom.Molec.Phys) 8, No.14, 2427, (1975).

GALANTI M, PEACOCK N J NORTON B A and PURIC J, Proc. Int. Conf. on Plasma Physics and Controlled Fusion, Tokyo, 1973. Publ IAEA Vienna 2 405 (1974).

GRIEM H R, "Spectral Line Broadening in Plasmas", Academic Press, London and New York, 1974.

GRIEM H R, BLAHA M and KEPPLE P C, Phys.Rev.A, 19 No.6, 2421 (1979).

HARES J D, KILKENNY J D, KEY M H and LUNNEY J G, Phys.Rev.Letts 42 No.18 1216, (1979).

HUGHES T P, Proc. 20th Scottish Universities Summer School in Physics (1979) "Laser Plasma Interactions". Edited by R A Cairns and J J Sanderson, St Andrews University.

IRONS F E, J.Phys.B. (Atom.Molec.Phys) 6 1562 (1973).

IRONS F E, Aust. J.Phys. 33 25 (1980).

KEY M H, Proc.20th Scottish Universities Summer School in Physics (1979) "Laser Plasma Interactions", Editor R A Cairns and J J Sanderson, St Andrews University.

KEY M H, EVANS R G, RUMSBY P T et al,Topical Meeting on Inertial Confinement Fusion, San Diego, 1980, paper WA7, publ. as Rutherford Laboratory Preprint RL-80-023

KEY M H, LEWIS C L S, LUNNEY J G, MOORE A, HALL T A and EVANS R G, Phys. Rev.Letts 41 No.21 1467, (1978).

KEY M H, LEWIS C L S, LUNNEY J G, MOORE A, WARD J M and THAREJA R K, Phys.Rev.Lett. 44, No.25, 1669, (1980).

KILKENNY J D, LEE R W, KEY M H, LUNNEY J G, Sub. Phys.Rev. (1979).

KRUER W L, Proc. 20th Scottish Universities Summer School in Physics, (1979) "Laser Plasma Interactions", edited by R A Cairns and J J Sanderson, St Andrews University.

LEE R W, BROMAGE G E and RICHARDS A G, J.Phys.B. (Atom.Molec.Phys) 12 No.20 3445 (1979).

LEE R W, J.Phys.B, 11, L167 (1978).

LEE R W and FREEMAN A J, Jnl.Quant.Spect. and Rad. Transfer. 24, 43 (1980).

LEE R W, I , J.Phys.B. 2, No.7, 1129, (1979).

LEE R W, II, J.Phys.B. 12, No.7, 1145, (1979).

LEE R W, III, J.Phys.B. 12, No.7, 1165, (1979).

LEWIS C L S, LAMB M J, WARD M J, CUNNINGHAM P and KILKENNY J D et al, Proc. 8th Int.Conf. on Plasma Phys and Contr. Nuc. Fusion Research, Brussels, 1980. Paper IAEA-CN-38/1-2. To be published IAEA Vienna.

MALVEZZI A M, FARIFO L, JANNITTI E, NICOLOSI P and TONDELLO G, J.Phys.B. (Atom.Molec.Phys) 12 No.8, 1437 (1979).

O'BRIEN J T and HOOPER C F, Phys.Rev. A5, No.2 867 (1972).

PEACOCK N J, Proc. Conf. on Phenomena in Ionised Gases, Berlin Vol.III, 383, Publ. Phys.Soc. of GDR 1977 - see also Culham Laboratory Report, CLM-P519 (1978).

PEACOCK N J, Proc. 20th Scottish Universities Summer School in Physics (1979), "Laser Plasma Interactions", Edited by R A Cairns and J J Sanderson, St Andrews University.

PEREGUDOV G V, RAGOZINE E N, SKOBELEV I Yu, VINOGRADOV A V and YUKOV E A, J.Phys.D, (Appl.Phys.) 11 2305 (1978).

ROZSNYAI B F, Jnl.Quant.Spectros.Rad.Transfer, 17, 77 (1976).

SMITH C C and PEACOCK N J, J.Phys.B(Atom.Molec.Phys) II, No.15, 2749 (1978).

SKUPSKY S, "Optically Thick Spectral Lines as a Diagnostic Tool for Laser-Imploded Plasmas", Laboratory for Laser Energetics, Report No.80, University of Rochester, USA (1978).

TALLENTS G J, J.Phys.B (Atom.Molec.Phys) 13, 3057 (1980).

TIGHE R J and HOOPER C F, Phys.Rev. A17 410 (1978).

VINOGRADOV A V, SOBELMAN I I and YUKOV E A, Kvant Elektron (Moscow) 1, 268 (1974).

YAAKOBI B, McCRORY R L, SKUPSKY S, DeLETTREZ J A et al, Optics Communications, 34, No.2, 213 (1980).

YAAKOBI B, SKUPSKY S, McCRORY R L, HOOPER C F et al, Phys.Rev.Letts, 44, No.16, 1072, (1980).

YAAKOBI B, STEEL D, THOROS E, HAUER A and PERRY B, Phys.Rev.Letts, 39 1526 (1977).

ZIGLER A, ZMORA H, LOEBENSTEIN H M, J.Appl.Phys. 50 (1) 165 (1979).